

Layer-dependent Electrocatalysis of MoS₂ for Hydrogen Evolution

Yifei Yu^{1§}, Shengyang Huang^{1§}, Yanpeng Li¹, Stephan Steinmann³, Weitao Yang³, Linyou Cao^{1,2*}

¹Department of Materials Science and Engineering, North Carolina State University, Raleigh NC 27695; ²Department of Physics, North Carolina State University, Raleigh NC 27695; ³Department of Chemistry, Duke University, Durham, NC 27708

§ These authors contribute equally.

*To whom correspondence should be addressed.

E-mail: lcao2@ncsu.edu

Abstract

The quantitative correlation of the catalytic activity with microscopic structure of heterogeneous catalysts is a major challenge for the field of catalysis science. It requests synergistic capabilities to tailor the structure with atomic scale precision and to control the catalytic reaction to proceed through well-defined pathways. Here we leverage on the controlled growth of MoS₂ atomically thin films to demonstrate that the catalytic activity of MoS₂ for the hydrogen evolution reaction decreases by a factor of ~4.47 for the addition of every one more layer. Similar layer dependence is also found in edge-riched MoS₂ pyramid platelets. This layer-dependent electrocatalysis can be correlated to the hopping of electrons in the vertical direction of MoS₂ layers over an interlayer potential barrier, which is found to be 0.119V and consistent with theoretical calculations. Our results point out that increasing the hopping efficiency of electrons in the vertical direction is a key for the development of high-efficiency two-dimensional material catalysts.

Seeking high-efficiency, cost-effective catalysts for mass production of hydrogen gas is critical for the utilization of hydrogen energy. The existing catalysts of Pt-group metals for the hydrogen evolution reaction (HER), which are highly efficient, are too expensive and rare to be useful for the mass production. Molybdenum disulfide (MoS_2) promises an earth-abundant, low-cost alternative to the precious metals¹. Considerable efforts have been dedicated to investigating and optimizing the catalytic activities of various MoS_2 materials, including nanoparticles²⁻⁴, nanopores⁵, nanowires⁶, amorphous and doped MoS_2 ⁷⁻⁹, thin films¹⁰, MoS_2 /graphene heterostructures¹¹, and chemically exfoliated MoS_2 layers¹²⁻¹⁵. It was suggested that the edge site and metallic 1T polymorph of MoS_2 materials are catalytically active^{2, 14-17}. However, despite the remarkable progress, the rational design of MoS_2 structures with optimal catalytic activities has remained elusive due to limited quantitative understanding on the correlation between the catalytic activity and microscopic structure of MoS_2 materials.

To quantitatively correlate the catalytic activity with microscopic structure requests capabilities to tailor the structure with atomic scale precision and to control the catalytic reaction to proceed in well-defined pathways. Most of the MoS_2 materials studied to date involve a wide dispersion in size, morphology, surface, and crystalline structure. This makes it difficult to assess the role of structural parameters in the catalytic performance. Here we demonstrate a layer-dependent electrocatalysis of MoS_2 for the HER by leveraging on a unique synthetic capability that can grow large-area, uniform, and high quality MoS_2 atomically thin films with precisely controlled layer numbers. The well-defined physical feature make the film an ideal platform for studies of the structure-catalysis correlation. We find that the catalytic activity, indicated by exchange current density, of the MoS_2 film decreases by a factor of about 4.47 for the addition of every one more layer. Similar layer dependence is also found in the electrocatalysis of edge-riched MoS_2 pyramid platelets. This layer-dependent electrocatalysis can be correlated to the hopping of electrons in the vertical direction of MoS_2 layers over an interlayer potential barrier, which is found to be 0.119V and consistent with theoretical calculations.

We grew MoS_2 thin films on glassy carbon substrates following a chemical vapor deposition (CVD) process that we previously developed¹⁸. The layer number was controlled by control of the amount of precursors (MoCl_5)¹⁸. The composition of the film was confirmed as MoS_2 by x-ray photoelectron spectroscopy (XPS) characterizations (Fig. S1). The synthesized films are continuous, uniform, and of high crystalline quality, similar to the films we previously grew on sapphire substrates¹⁸. It can be seen uniformly covering the entire substrate under optical microscopes (Fig. 1a and Fig. S2). Atomic force microscope (AFM) characterizations identify the synthesized monolayer, bilayer, and trilayer MoS_2 films in thickness of 0.90 nm, 1.70 nm and 2.15 nm, respectively (Fig. 1b and Fig. S3). These measured results are slightly larger than those of the MoS_2 films grown on sapphire¹⁸, which may be related with the relatively larger surface roughness of the glassy carbon substrate (~ 1 nm) than that of sapphire. Raman measurements can further confirm the layer number. The frequency differences (Δk) of the two characteristic Raman modes (A_{1g} and E_{2g}^1 modes), which is widely used to identify the layer number¹⁹, of the synthesized monolayer, bilayer, and trilayer MoS_2 films are 20.5, 22.4, and 23 cm^{-1} (Fig. 1c), respectively, consistent with previous results^{18, 19}. The AFM and Raman characterizations also confirm the large-area continuity and uniformity of the synthesized films. No substantial voids, steps, and edges were found in the films through numerous AFM measurements. And the frequency difference Δk remains reasonably constant during extensive Raman characterizations

across the films (Fig. S4). Additionally, the crystalline quality of the synthesized films is reasonably high, as evidenced by the full width at half maximum (FWHM) of the E_{2g}^1 mode that is known related with crystalline quality¹⁹. The E_{2g}^1 FWHM of these MoS₂ films is comparable with the MoS₂ films grown on sapphire, which we previously demonstrated in high crystalline quality by electron microscope and electrical/optical characterizations (Fig.S5)¹⁸.

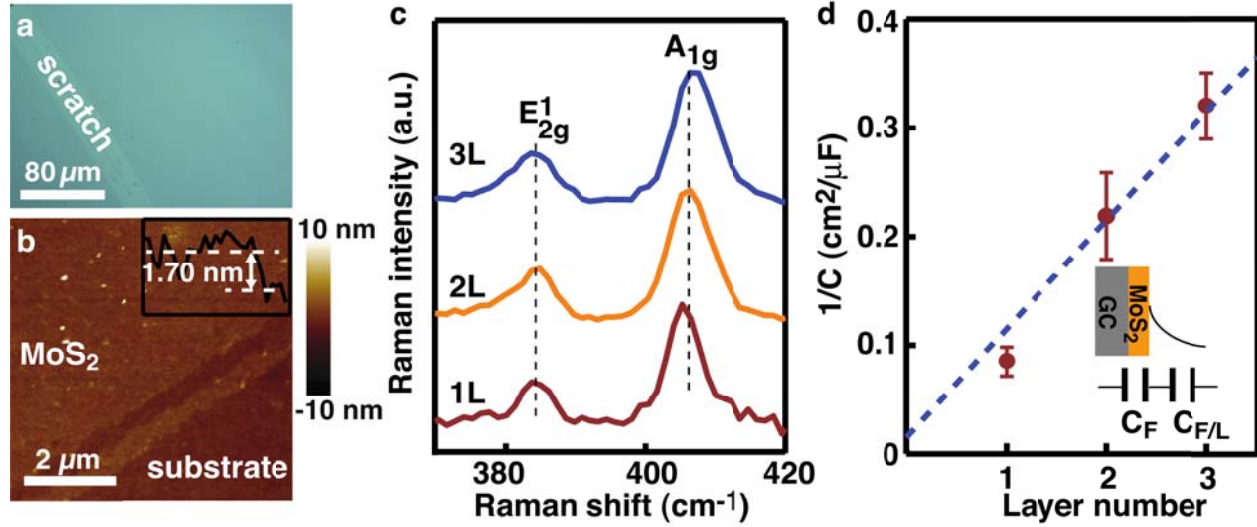


Fig.1. Structure characterizations of the synthesized MoS₂ films. (a) Optical image and (b) AFM image of a bilayer MoS₂ film (monolayer and trilayer see Fig. S1 and S3). A scratch is intentionally made in the film to show the contrast between the substrate and the film and for the convenience of characterizing the height of the film. The inset of (b) is a typical height profile of the film. (c) Raman spectra of the synthesized monolayer (1L), bilayer (2L), and trilayer (3L) MoS₂ films. The dashed lines serve to visualize the layer-dependent Raman shift. The characteristic Raman modes are labeled as shown. (d) The reciprocal of measured capacitances of the films as a function of the layer number. Inset is a schematic illustration for the model of two capacitors in series.

The layer number of the film can be confirmed by capacitance measurements. The reciprocal of the measured capacitance ($1/C$) of the film is found linearly dependent on the layer number (Fig. 1d). This linear dependence can be accounted by a model of two capacitors in series, the film with a capacitance of C_F and the double-layer at the film/liquid interface with a capacitance of $C_{F/L}$, $1/C = 1/C_F + 1/C_{F/L}$ (Fig. 1d inset). C_F is dependent on the thickness d and dielectric constant of the MoS₂ film ϵ_r , $C_F = \epsilon_r \epsilon_0 / d$ (ϵ_0 is the vacuum permittivity). By linearly fitting the measured capacitance with the model, we can find out the double-layer capacitance $C_{F/L}$ as 66.7 μF/cm², similar to the typical double-layer capacitances previously reported⁵. We can also find the capacitance of monolayer MoS₂ C_F as 10 μF/cm². This suggests the dielectric constant of MoS₂ monolayers ϵ_r to be 7.63, consistent with the result in reference²⁰.

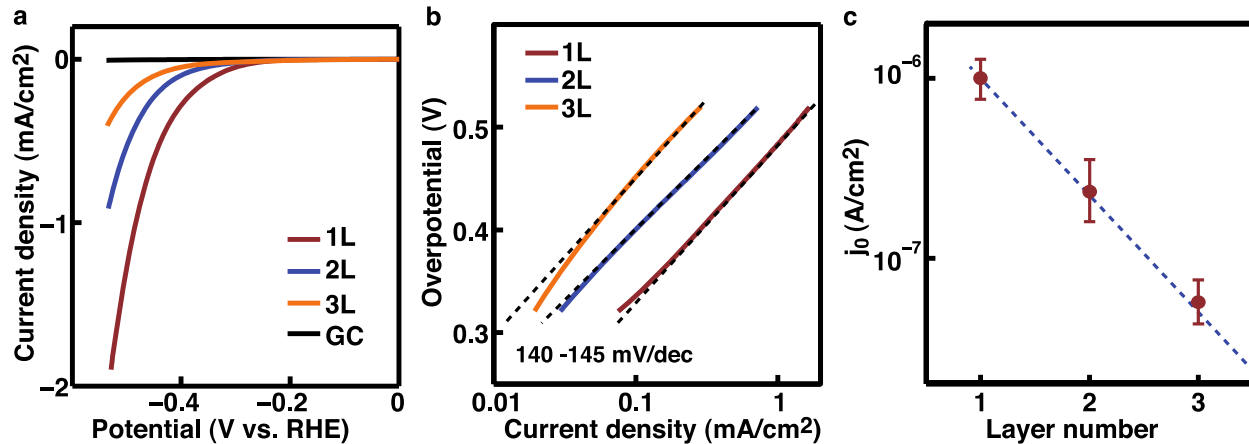


Fig. 2. Layer dependence of the catalytic activities of MoS₂ films. (a) Polarization curves of the synthesized monolayer (red, 1L), bilayer (blue, 2L), and trilayer (orange, 3L) MoS₂ films. The curve of bare glass carbon substrates is also given (black). (b) Tafel plots of the MoS₂ films. The dashed lines are linear fitting for the plots. (c) The exchange current density of the MoS₂ film as a function of the layer number. The current density is plotted in a logarithmic scale. The dashed line is a fitting of $\log j_0 = -0.65x - 5.35$.

The electrocatalysis of the MoS₂ film strongly depends on the layer number. Fig. 2a-b shows the polarization curves and corresponding Tafel plots of the synthesized monolayer, bilayer, and trilayer films. The polarization curve of bare glassy carbon electrodes is also given in Fig. 2a, whose trivial current indicates that the glassy carbon is catalytically inactive for the HER. From these results we can find that the cathodic current of the film monotonically decreases with the layer number increasing.

The observed layer dependence can be linked to exchange current densities. By fitting the Tafel plots to the equation of $\eta = \rho \log j + \log j_0$ (overpotential η , current density j , and exchange current density j_0), we can find that all the films have a similar slope ρ in the range of 140 – 145 mV/decade, while the exchange current density j_0 substantially decreases with the layer number increasing. We repeated the electrocatalytic characterization with numerous MoS₂ films (>15 films in total). The results reproducibly show a constant ρ in the range of 140-145 mV/decade and a layer-dependent j_0 (Fig. 2c). Interestingly, j_0 decreases by a factor of ~ 4.47 for the addition of every one more layer. Note that the observed Tafel slope is larger than typical results on MoS₂ materials. This may be related with the high temperature (850°C) used in the synthetic process. Other groups reported a slope of ~ 120 mV/decade in the MoS₂ materials processed at a temperature of ~ 500 °C^{10, 14, 15}, and it has been well known that a processing of MoS₂ materials at a higher temperature can result in a higher Tafel slope^{10, 14-16, 21}. As will be shown later (Fig. 4), similar Tafel slopes (~ 140 mV/decade) can be found in the other MoS₂ structures (i.e. edge-riched pyramid platelets) synthesized at the same temperature (850°C). This indicates that the Tafel slope is not related with the structure of the film that is of our major interest in this work.

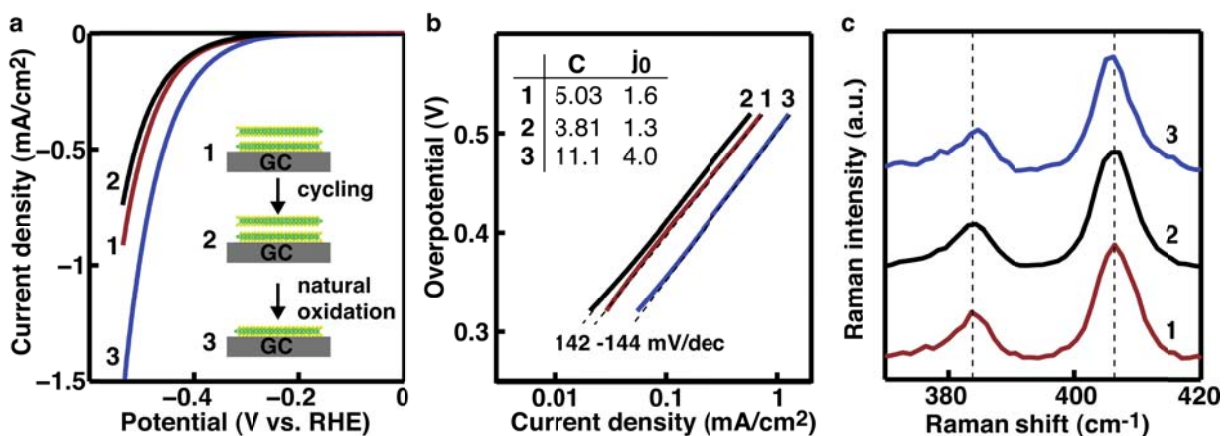


Fig. 3. Improvement in the electrocatalysis of MoS₂ films after the stripping process. (a) Polarization curves of a bilayer MoS₂ film recorded at the different stages in the stripping process: 1, as-grown, 2, after cyclic voltammetry, and 3, after oxidation and dissolution. Inset, schematic illustration for the stripping process. (b) Tafel plots corresponding to the results in (a). The dashed lines indicate the linear fitting for the slope. Inset lists the capacitance (C , $\mu\text{F}/\text{cm}^2$) and exchange current density (j_0 , $10^{-7} \text{ A}/\text{cm}^2$) of the bilayer film at the different stages. (c) Raman spectra of the bilayer MoS₂ film at the different stages. The dashed lines serve to visualize the change in the Raman spectra.

The layer-dependent electrocatalysis can be confirmed by a substantial improvement in the catalytic activities of bilayer and trilayer MoS₂ films after a stripping process. The stripping process is designed to selectively strip off the outmost layer of the film (Fig. 3 and Fig. S6). It involves procedures of cyclic voltammetry (CV), natural oxidation, and dissolution. We first performed multiple (> 1000 times) CV with the film in a potential range (+0.2 to -0.3V) smaller than the range for the electrocatalysis measurement (+0.2 to -0.6V), and then naturally exposed the CV-processed film to air for weeks (typically one month), which was followed by an immersion of the film into electrolyte solutions. We believe that the outmost layer of the CV-processed film can be gradually oxidized into Mo⁶⁺ (for instance, MoO₃) by the exposure to air, and that the oxidized layer can be dissolved in aqueous solutions to expose the layer underneath due to a weak solubility of MoO₃ in water. This stripping mechanism is confirmed by our XPS characterizations through the process. The XPS characterization shows no oxidation (Mo⁶⁺) in the film right after the CV processing, but substantial oxidation (Mo⁶⁺) can be found after the CV-processed film being exposed to air for one month. The oxidation (Mo⁶⁺) peak can be found disappearing again after the oxidized film being immersed into the electrolyte solution (Fig. S7). This indicates that the CV processing does not oxidize the film but may somehow cause it easier to be oxidized by air. The XPS results also indicate that the ratios of Mo⁶⁺ and Mo⁴⁺ are around 1:0, 1:1, and 1:2 in the monolayer, bilayer and trilayer films respectively after the natural oxidation (Fig. S8). This suggests that the electrochemical reaction only occurs at the outmost layer, which subsequently limits the oxidation at that layer.

Fig. 3a-b shows the polarization currents and corresponding Tafel plots of a bilayer film recorded through the stripping process (results for the other films see Fig. S6). The current slightly decreases after the CV processing (curve 2 in Fig. 3a) but turns to be much stronger than the initial value after the stripping (curve 3 in Fig. 3a). While the Tafel slope remains pretty

much constant through the process, the exchange current density substantially increases from 1.6×10^{-7} to 5×10^{-7} A/cm² after the stripping (Fig. 3b). Capacitance and Raman measurements both confirm that the bilayer film indeed becomes a monolayer after the stripping, the capacitance changing from 5.08 to 11.1 μ F/cm² (Fig. 3b inset) and the frequency Δk from 22.4 cm⁻¹ (curve 1 in Fig. 3c) to 20.5 cm⁻¹ (curve 3 in Fig. 3c). It is worthwhile to note no obvious change in the Raman spectrum collected right after the CV processing (curve 2 in Fig. 3c). This confirms that the electrochemical process does not cause substantial changes in the structure and composition of the film. Similar increase in the catalytic activity after the stripping process can also be found in trilayer MoS₂ films, but understandably not in monolayer MoS₂ films (Fig. S6).

It is important to understand the mechanism underlying the observed layer-dependent exchange current density. We can reasonably exclude differences in the composition (i.e. stoichiometry) and crystalline quality (i.e. defects) of the MoS₂ films, which might cause difference in the electrocatalysis, because all of them were grown under highly comparable conditions. Additionally, previous studies show that the exchange current density of MoS₂ materials linearly depends on the number of edge sites¹⁶. However, we can exclude the difference in the number of edge sites as the cause for the layer-dependent exchange current densities. The synthesized MoS₂ films are continuous, uniform, and show reasonably high crystalline quality (Fig.1). It is safe to conclude that there is no substantial amount of edge sites in the synthesized films and the observed layer dependence is related with the MoS₂ atoms in the basal plane.

To further support that the number of edge sites is not the cause, we grew MoS₂ pyramid platelets on glassy carbon substrates using temperatures similar to what were used for the synthesis of the film and tested the electrocatalytic performance of the platelets. The synthesized platelets show a monodisperse distribution in size (Fig. 4a lower inset). Different from the film, in which no obvious edges can be found, the pyramid platelet consists of a large number of gradually-shrinking monolayers stacking in the vertical direction with a rich amount of edge sites exposed (Fig. 4a-b). We can find that the pyramid platelets show a very poor electrocatalytic performance (Fig. 4c). The Tafel slope, ~ 140 mV/decade, is similar to what was observed in the film. As discussed in the preceding text, this is related with the synthetic temperature and is not our interest here. The exchange current density, 0.6×10^{-7} A/cm², is barely comparable to those of trilayer thin films. The poor performance of the edge-riched platelets indicates that the number of edge sites is not the cause for the observed layer dependence. Otherwise, we would expect a high exchange current density in the platelets.

Our experimental results also suggest a layer dependence in the electrocatalysis of the edge-riched platelets. We observed the catalytic performance of the pyramid platelets increasing with the size decreasing (Fig. S9). The ratio between the size and height of the pyramid platelet always remains to be constant around 60 (Fig. S9). This constant size/height ratio can enable comparable number of edge sites in unit area among the platelets in different sizes. Therefore, the observed sized-dependent electrocatalysis of the platelet can be ascribed to a dependence on the layer number (height), instead of the density of edge sites. The layer dependence can account for the poorer performance observed in the platelets with a larger height (Fig. 4c). Only the part closed to the substrate electrode can effectively participate the catalytic reaction.

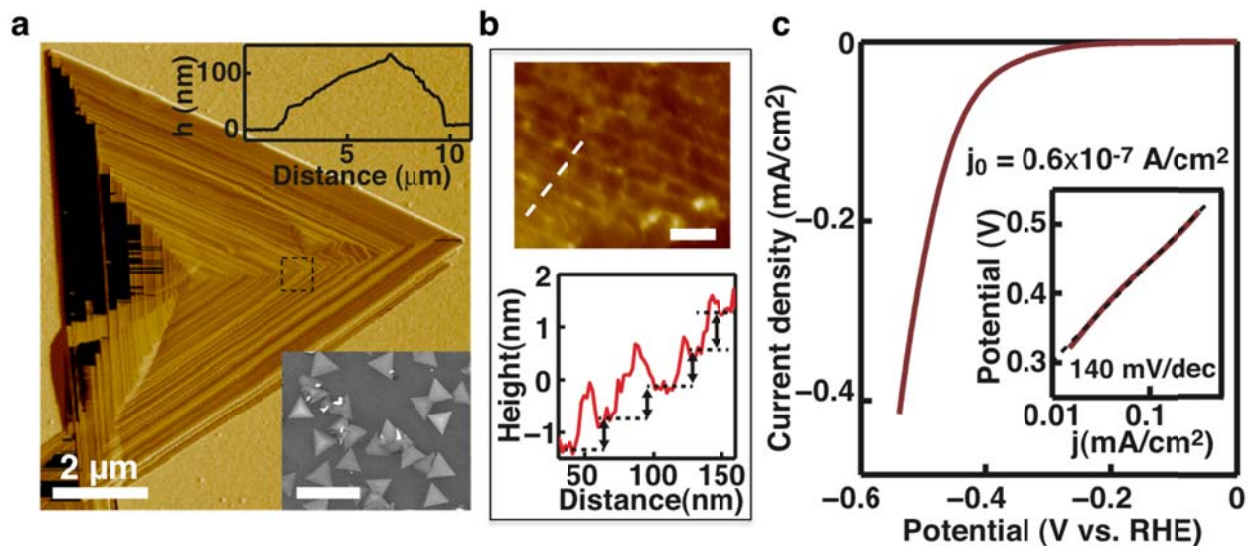
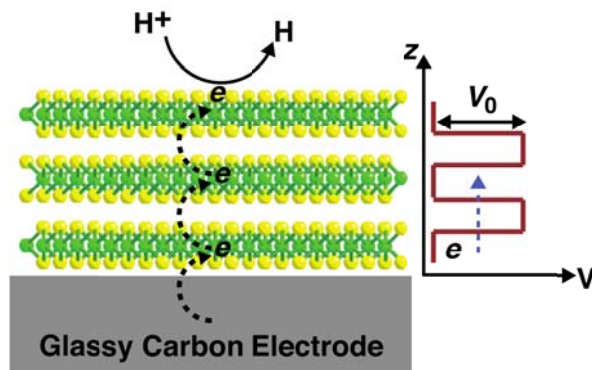


Fig. 4. Poor electrocatalytic performance of edge-rich MoS₂ pyramid platelets. (a) AFM image of a typical pyramid. Low inset, SEM image of the platelets on glass carbon substrates with a scale bar of 20 μm ; upper inset, a typical height profile for the platelet. (b) A magnified image of the area indicated by the dashed square in (a) as well as the height profile for the given dashed white line. The arrows shown in the height profile indicate that the step is one layer. Scale bar, 100 nm. (c) Polarization curve and Tafel plot of the MoS₂ pyramid platelet. The given current density considers is normalized to the area of the platelets by considering the partial coverage (60%) of the platelets on the substrate. The Tafel slope and exchange current density are noted as shown.

We find that the layer-dependent exchange current density can be correlated to the hopping of electrons in the vertical direction of MoS₂ layers. As discussed in the preceding text, our results indicate that the electrochemical reaction only occurs at the outmost layer of the film. Electrons have to transfer from the glassy carbon electrode to the outmost layer in order to drive the HER (Fig. 4). It is known that the electron transfer in the direction perpendicular to the basal plane of MoS₂ materials is through hopping²², because potential barriers exist in the interlayer gap. We can build up a quantum-tunneling model for the hopping process (Fig. 4). The hopping efficiency is dictated by the interlayer distance L and the potential barrier V_0 as $T = e^{-2kL}$, and $k = (2m_e V_0)^{1/2}/\hbar$, where m_e is the effective mass of electrons and \hbar is the Planck's constant. Our results, the exchange current density decreasing by a factor of 4.47 for the addition of every one more layer, suggest $T = e^{-2kL} = 1/4.47$. By substituting the values of L (0.62 nm) and m_e ($0.48m_0$, $m_0 = 9.11 \times 10^{-31}$ kg) in MoS₂ atomic films²³, we can get $V_0 = 0.119$ V. This value is in excellent consistence with a recent theoretical calculation, which predicts that the hopping potential in the vertical direction of MoS₂ layers is 0.123 V²⁴. The nice consistence suggests a dominant role of the electron hopping in the layer-dependent electrocatalysis of MoS₂.

We have demonstrated a layer-dependent electrocatalysis of MoS₂ materials and elucidate that the layer dependence is dictated by the interlayer hopping of electrons. The layer dependence is found in both MoS₂ atomically thin films, which has little edge sites, and edge-rich structures. Different from conventional wisdom, which think the edge site is catalytically active, our results suggests that the atoms in the basal plan can be active sites for catalysis as well. The reportedly

better catalytic performance of the edge sites could be because the edge site provides a better way to transfer the electron than the atoms in the basal plane. Our results suggest that increasing the hopping efficiency of electrons is a key for the rational design of MoS₂ materials with optimal catalytic activities. The efficiency of hopping is reportedly determined by the interlayer coupling of electron orbitals²⁴. Therefore, strategies that can increase the interlayer coupling, such as intercalation of metal ions or atoms, are expected able to enhance the electrocatalytic performance of MoS₂ materials.



Methods

1. Synthesis of MoS₂ atomic films with controlled layer number

MoS₂ thin films were synthesized in a tube furnace following a chemical vapor deposition process we have recently developed¹⁸. In a typical growth, 1-50 mg of molybdenum chloride (MoCl₅) powder (99.99%, Sigma-Aldrich) was placed at the center of the furnace and 1g of sulfur powder (Sigma-Aldrich) were placed at the upstream entry of the furnace. Receiving substrates (glassy carbon) were placed in the downstream of the tube. Typical conditions for MoS₂ thin film growth included a temperature of 850 °C, a flow rate of 50 sccm, and a pressure around 2 Torr. The precursors were subjected to evaporation at elevated temperatures. The vapor of the precursor materials reacted to produce gaseous MoS₂ species, which could subsequently precipitate onto receiving substrates at downstream to yield MoS₂ films. The layer number of the synthetic MoS₂ thin film can be controlled by control of the amount of MoCl₅ precursor. More details can be seen in Ref. 18. MoS₂ pyramid platelets were grown with similar conditions as what were used for the growth of thin films. The only difference lies in the pressure. 760 Torr was used for the growth of the pyramid platelets.

2. Structure and electrochemical characterizations

The structure and composition of the synthesized films were characterized by tools including optical microscope, atomic force microscope (AFM), Raman spectroscopy, and X-ray photoelectron spectroscopy (XPS). AFM measurements were performed with a Veeco Dimension-3000 AFM. Raman spectra were collected on a Renishaw-1000 Raman spectroscopy with an excitation wavelength of 514.5 nm. XPS were performed on a SPECS System with PHOIBOS 150 Analyzer using an Mg K α X-ray source.

The electrochemical characterization of the MoS₂ films were performed in 0.5 M H₂SO₄ using a CH Instrument electrochemical analyzer (Model CHI604D), a Pt-wire counter electrode, a

saturated calomel reference electrode (SCE), and a glassy carbon (0.785 cm^2) working electrode. Nitrogen gas was bubbled into the electrolyte throughout the experiment. While all the electrochemical characterization studies were performed using a saturated calomel reference electrode (SCE), the potential values mentioned in the electrochemical study are referred to a reversible hydrogen electrode (RHE). Calibration of the reference electrode for the reversible hydrogen potential was performed using a platinum (Pt) disk as working electrode and a Pt wire as counter electrode in $0.5\text{ M H}_2\text{SO}_4$. The electrolyte was purged with ultrahigh purity hydrogen (Airgas) during the measurement. The potential shift of the SCE is -0.262 V vs. RHE. The electrocatalysis was measured using linear sweeping from $+0.2\text{ V}$ to -0.6 V (vs. RHE) with a scan rate of 5 mV/S . The cycling voltammetry was performed in a range of $+0.2$ to -0.3 V (vs. RHE) at a scan rate of 50 mV/s .

The capacitance of the film was characterized using electrochemical impedance spectroscopy (EIS). The AC impedance is measured within the frequency range of 10^5 to 1 Hz with perturbation voltage amplitude of 5 mV . An equivalent Randles circuit model was fit to the data with ZSimpWin software to determine the system resistance and the capacitance.

Acknowledgement

L. C. acknowledges a Young Investigator Award from the Army Research Office (W911NF-13-1-0201).

Author Contributions

Y. Y. and L. C. conceived the experiments. Y. Y., S. H., and Y. L. performed the experiments. Y. Y., S. H., and L.C. analyzed the data. S. S., W. Y., and L. C. came up the mechanism. All authors were involved in writing the manuscript.

Competing financial interests

The authors declare no competing financial interests.

References

1. Laursen, A.B., Kegnaes, S., Dahl, S. & Chorkendorff, I. Molybdenum sulfides-efficient and viable materials for electro - and photoelectrocatalytic hydrogen evolution. *Energ Environ Sci* **5**, 5577-5591 (2012).
2. Hinnemann, B. et al. Biomimetic hydrogen evolution: MoS₂ nanoparticles as catalyst for hydrogen evolution. *J Am Chem Soc* **127**, 5308-5309 (2005).
3. Vrubel, H., Merki, D. & Hu, X.L. Hydrogen evolution catalyzed by MoS₃ and MoS₂ particles. *Energ Environ Sci* **5**, 6136-6144 (2012).
4. Bonde, J., Moses, P.G., Jaramillo, T.F., Norskov, J.K. & Chorkendorff, I. Hydrogen evolution on nano-particulate transition metal sulfides. *Faraday Discuss* **140**, 219-231 (2008).
5. Kibsgaard, J., Chen, Z.B., Reinecke, B.N. & Jaramillo, T.F. Engineering the surface structure of MoS₂ to preferentially expose active edge sites for electrocatalysis. *Nat Mater* **11**, 963-969 (2012).
6. Chen, Z.B. et al. Core-shell MoO₃-MoS₂ Nanowires for Hydrogen Evolution: A Functional Design for Electrocatalytic Materials. *Nano Lett* **11**, 4168-4175 (2011).
7. Merki, D., Fierro, S., Vrubel, H. & Hu, X.L. Amorphous molybdenum sulfide films as catalysts for electrochemical hydrogen production in water. *Chem Sci* **2**, 1262-1267 (2011).
8. Merki, D., Vrubel, H., Rovelli, L., Fierro, S. & Hu, X.L. Fe, Co, and Ni ions promote the catalytic activity of amorphous molybdenum sulfide films for hydrogen evolution. *Chem Sci* **3**, 2515-2525 (2012).
9. Benck, J.D., Chen, Z., Kuritzky, L.Y., Forman, A.J. & Jaramillo, T.F. Amorphous Molybdenum Sulfide Catalysts for Electrochemical Hydrogen Evolution: Insights into the Origin of their Catalytic Activity. *ACS Catalysis* **2**, 1916-1923 (2012).
10. Kong, D.S. et al. Synthesis of MoS₂ and MoSe₂ Films with Vertically Aligned Layers. *Nano Lett* **13**, 1341-1347 (2013).
11. Li, Y.G. et al. MoS₂ Nanoparticles Grown on Graphene: An Advanced Catalyst for the Hydrogen Evolution Reaction. *J Am Chem Soc* **133**, 7296-7299 (2011).
12. Huang, X. et al. Solution-phase epitaxial growth of noble metal nanostructures on dispersible single-layer molybdenum disulfide nanosheets. *Nat Commun* **4** (2013).
13. Chhowalla, M. et al. The chemistry of two-dimensional layered transition metal dichalcogenide nanosheets. *Nat Chem* **5**, 263-275 (2013).
14. Lukowski, M.A. et al. Enhanced Hydrogen Evolution Catalysis from Chemically Exfoliated Metallic MoS₂ Nanosheets. *J. Am. Chem. Soc.* **135**, 10274-10277 (2013).
15. Voiry, D. et al. Enhanced catalytic activity in strained chemically exfoliated WS₂ nanosheets for hydrogen evolution. *Nat. Mater.* **12**, doi:10.1038/nmat3700 (2013).
16. Jaramillo, T.F. et al. Identification of active edge sites for electrochemical H₂ evolution from MoS₂ nanocatalysts. *Science* **317**, 100-102 (2007).
17. Karunadasa, H.I. et al. A Molecular MoS₂ Edge Site Mimic for Catalytic Hydrogen Generation. *Science* **335**, 698-702 (2012).
18. Yu, Y.F. et al. Controlled Scalable Synthesis of Uniform, High-Quality Monolayer and Few-layer MoS₂ Films. *Sci Rep-Uk* **3** (2013).

19. Lee, C. et al. Anomalous Lattice Vibrations of Single- and Few-Layer MoS₂. *Acs Nano* **4**, 2695-2700 (2010).
20. Frindt, R.F. & Yoffe, A.D. Physical Properties of Layer Structures - Optical Properties and Photoconductivity of Thin Crystals of Molybdenum Disulphide. *Proc R Soc Lon Ser-A* **273**, 69-+ (1963).
21. Chang, Y.-H. et al. Highly Efficient Electrocatalytic Hydrogen Production by MoS_x Grown on Graphene-Protected 3D Ni Foams. *Adv Mater* **25**, 756-760 (2012).
22. Tang, H. & Morrison, S.R. Optimization of the Anisotropy of Composite Mos₂ Films. *Thin Solid Films* **227**, 90-94 (1993).
23. Cheiwchanchamnangij, T. & Lambrecht, W.R.L. Quasiparticle band structure calculation of monolayer, bilayer, and bulk MoS₂. *Phys Rev B* **85** (2012).
24. Cappelluti, E., Roldan, R., Silva-Guillen, J.A., Ordejon, P. & Guinea, F. Tight-binding model and direct-gap/indirect-gap transition in single-layer and multi-layer MoS₂. *arXiv: 1304.4831* (2013).

*Supplementary Materials
for*

Layer-dependent Electrocatalysis of MoS₂ for Hydrogen Evolution

Yifei Yu^{1§}, Sheng-Yang Huang^{1§}, Yanpeng Li¹, Stephan N. Steinmann³,
Weitao Yang³, Linyou Cao^{1,2*}

¹Department of Materials Science and Engineering, North Carolina State University, Raleigh NC 27695; ²Department of Physics, North Carolina State University, Raleigh NC 27695;

³Department of Chemistry, Duke University, Durham, NC 27708

§ These authors contribute equally.

*To whom correspondence should be addressed.

E-mail: lcao2@ncsu.edu

This PDF document includes

Fig. S1-S9

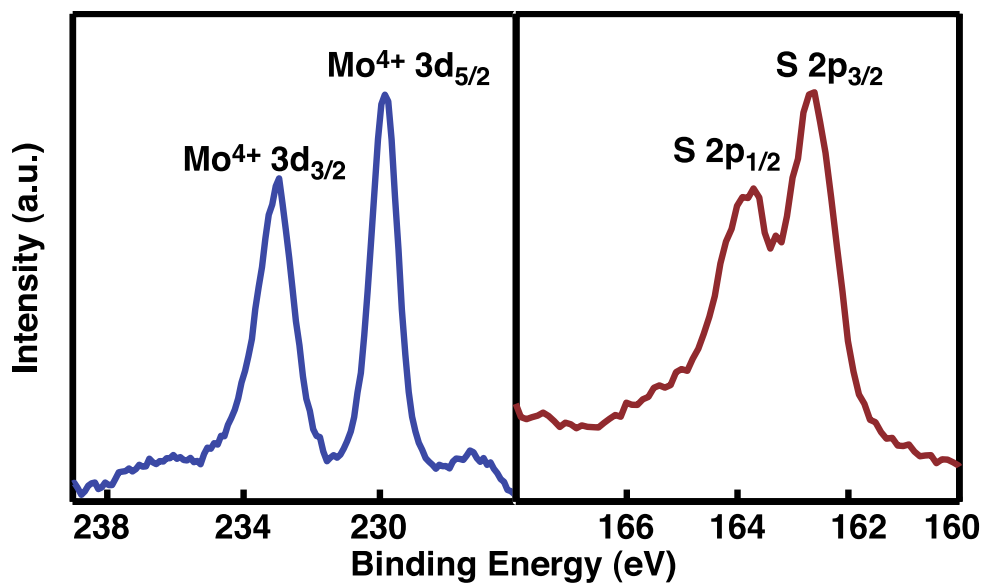


Fig. S1. XPS of the synthesized MoS_2 films. Binding energies for (**Left**) the Mo atoms and (**Right**) the sulfur atoms. The XPS peaks are assigned as shown.

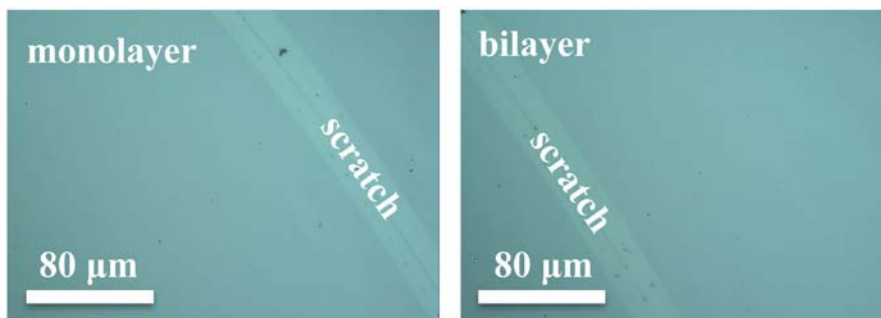


Fig.S2. Optical images of monolayer and bilayer MoS_2 films grown on glassy carbon substrates. Scratches (brighter regions) are intentionally introduced in the films to show the color contrast between the substrate and the film. We can see that the bilayer is a little bit darker than the monolayer.

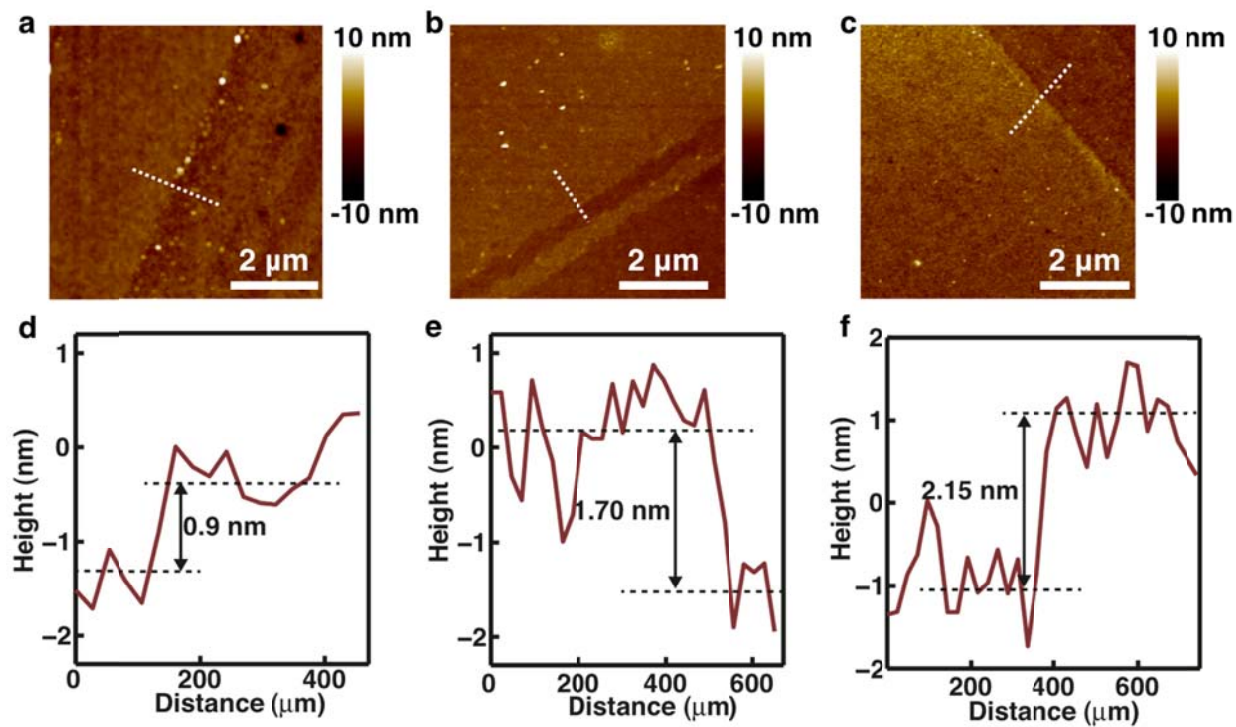


Fig. S3. AFM characterizations. (a-c) Typical AFM images of the synthesized monolayer, bilayer, and trilayer films grown on glassy carbon substrates. The area occupied by the MoS_2 is labeled as shown. (d-f) Height profiles for the white dashed lines shown in (a-c), respectively.

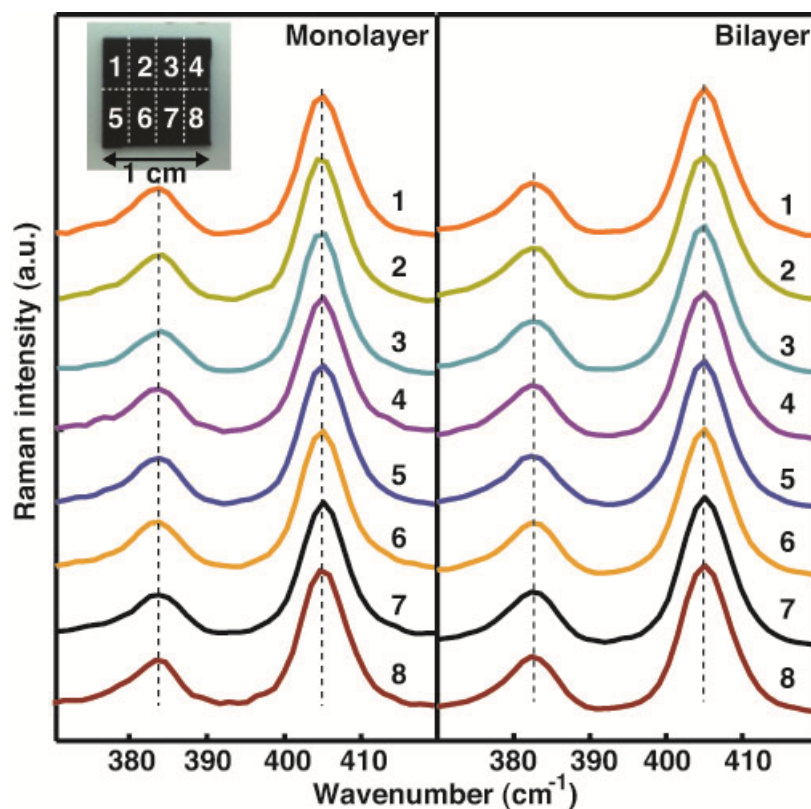


Fig. S4. Raman spectra collected from numerous locations of the MoS₂ film. Eight of the collected Raman spectra for the monolayer and the bilayer are given as shown. The inset schematically shows the eight spectra collected from locations evenly distributing across the film. The dashed lines serve to visualize the constant Raman peaks across the entire film.

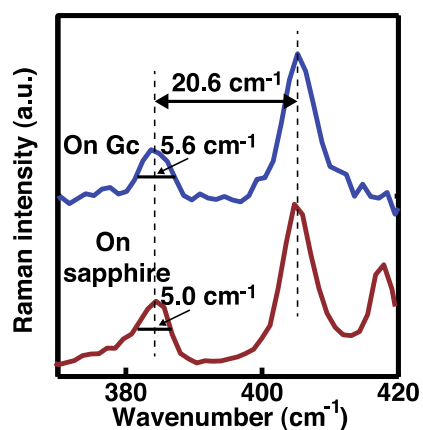


Fig. S5. Raman spectra of the monolayer MoS₂ films grown on the substrates of glassy carbon (GC, blue) and sapphire (red). The frequency difference between the two characteristic Raman modes of MoS₂ is given. Also given is the full width at half magnitude (FWHM) of the E_{2g}¹ mode ($\sim 385 \text{ cm}^{-1}$) in the films.

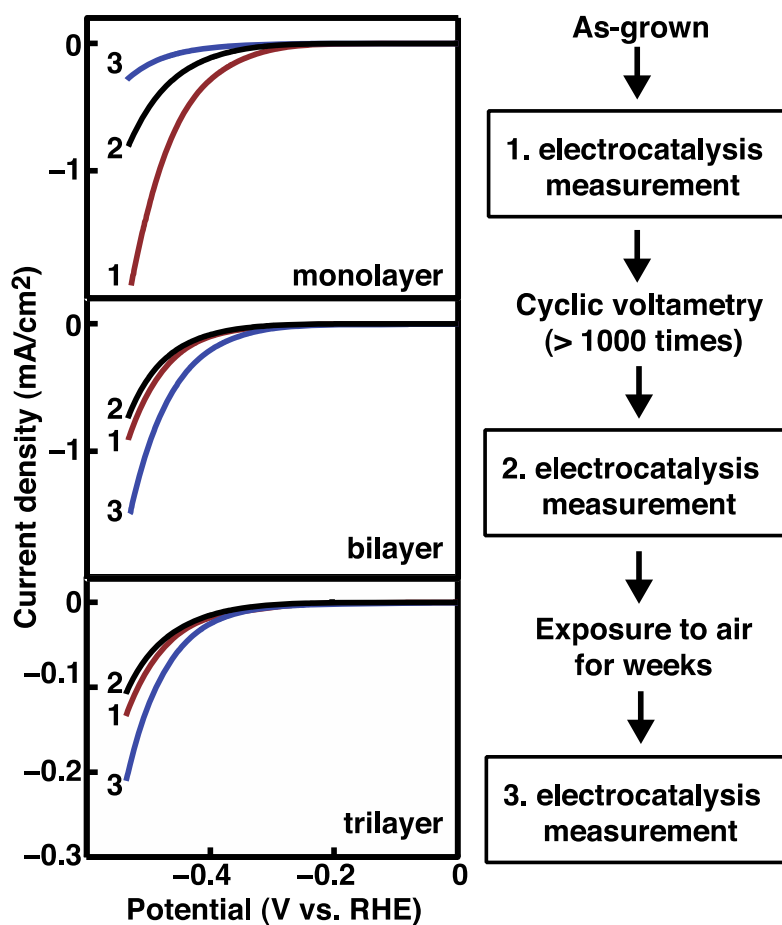


Fig.S6. Polarization curves of the MoS₂ films in the stripping test. The polarization curves of the monolayer, bilayer, and trilayer MoS₂ films were recorded at different stages of the stripping test. The diagram to the right illustrates the different stages, 1. as-grown films, 2, after the cyclic voltammetry processing, and 3. After exposing the CV-process films to air for weeks.

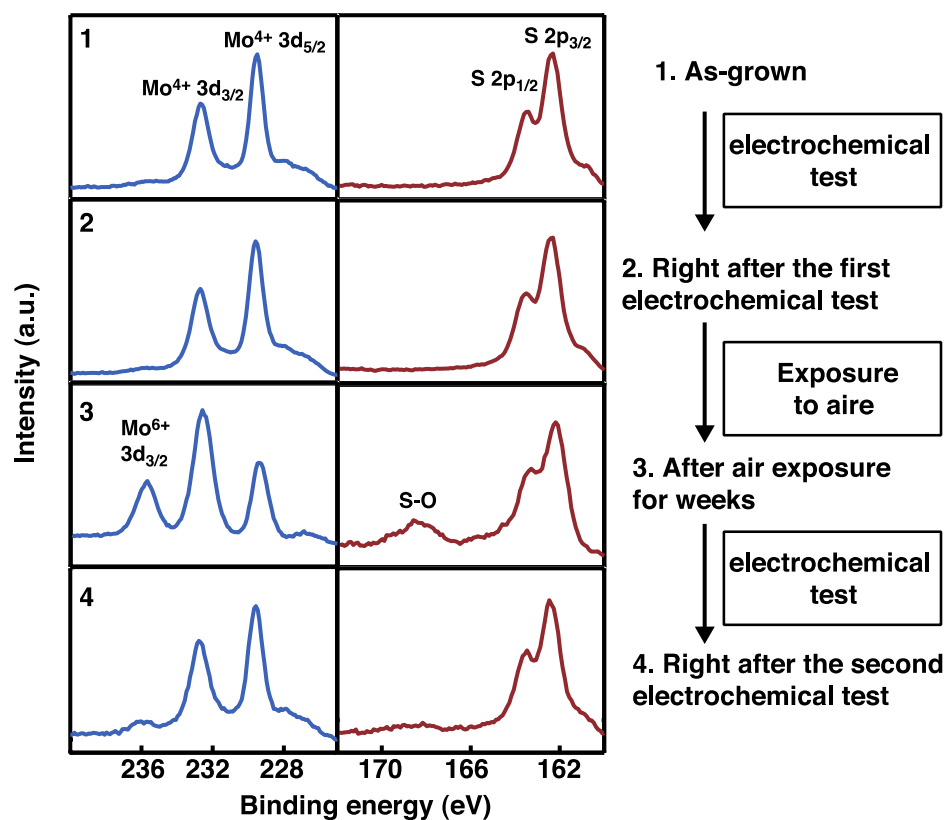


Fig. S7. XPS characterization of the MoS₂ films through the stripping test. The composition of the MoS₂ film was monitored at the different states through the stripping test. Both the binding energy of (**Left**) the Mo atoms and (**Middle**) the sulfur atoms are given. The diagram to the right illustrates the different stages, 1. as-grown films, 2, after the cyclic voltammetry processing, 3. after exposing the CV-process films to air for weeks, and 4, after immersing the air-exposed films into electrolyte solutions.

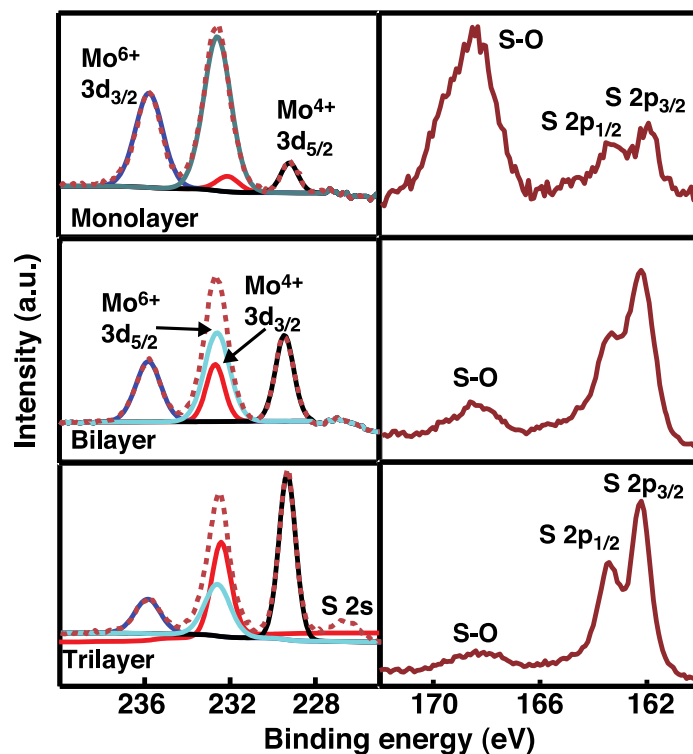


Fig. S8. XPS characterization of the oxidation in MoS₂ films. The XPS characterizations were performed with the monolayer, bilayer, and trilayer MoS₂ film after the CV processing and exposure to air for weeks. Both the binding energy of (Left) the Mo atoms and (Middle) the sulfur atoms are given. The XPS peaks are assigned as shown. Curve fitting was performed for the results of Mo atoms in order to find out the ratio of Mo⁶⁺ and Mo⁴⁺, which is demonstrated as 89.7:10.3, 51.73:48.27, and 33.91:66.09 for the monolayer, bilayer, and trilayer films, respectively.

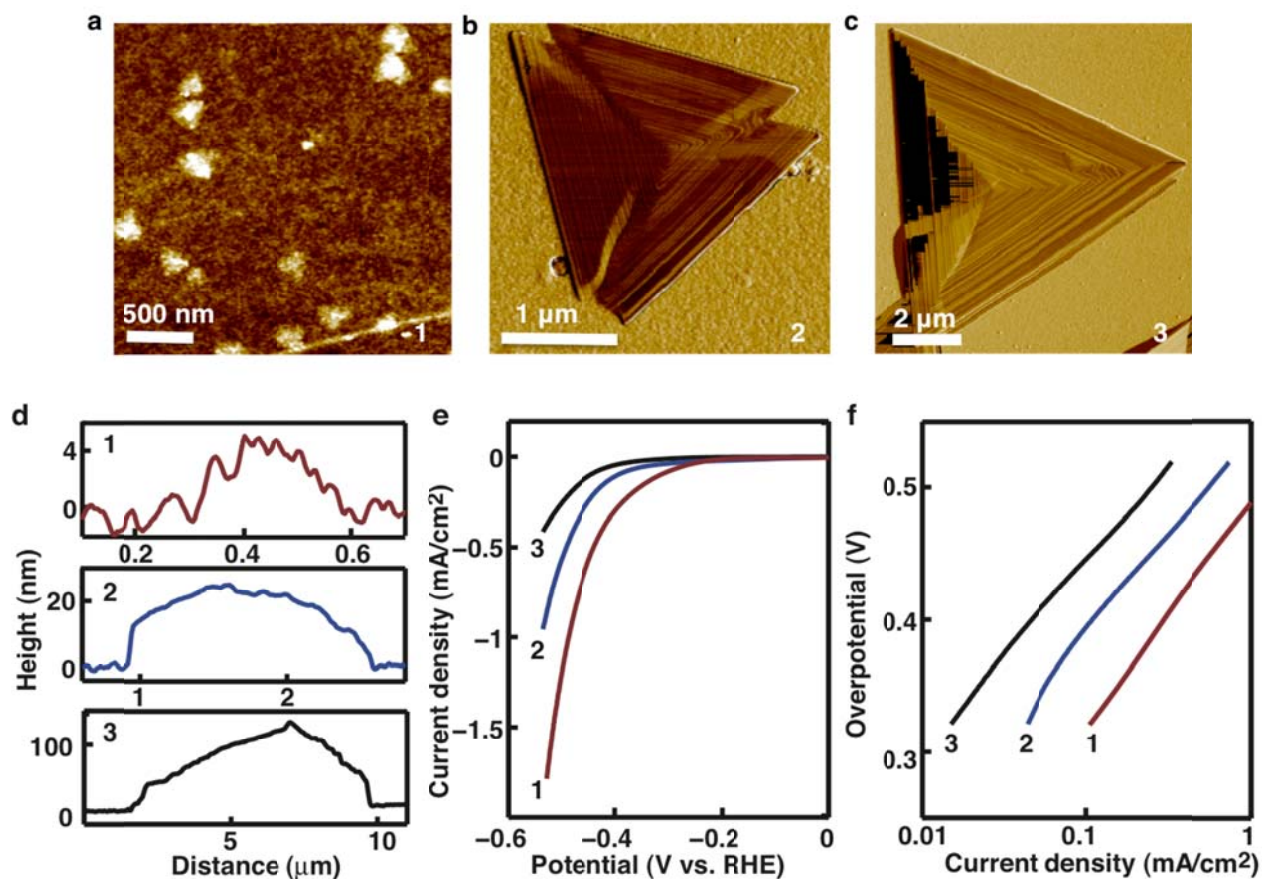


Fig. S9. Characterizations of MoS₂ pyramid platelets grown on glassy carbon substrates. (a-c) AFM images of MoS₂ pyramid platelets with different sizes. For the convenience of discussion, each of these platelets is assigned with a number, 1, 2, and 3, respectively. (d) Typical height profile obtained from AFM characterizations of the three types of platelets. (e-f) Typical polarization curves and corresponding Tafel plots of the triangle platelets.